phys. stat. sol. (c) **1**, No. 6, 1511–1521 (2004) / **DOI** 10.1002/pssc.200304095

Electronic and optical properties of [N11] grown nanostructures

Michael Povolotskyi[*, 1], **Aldo Di Carlo**[1], and **Stefan Birner**[2]

[1] Dept. of Electronic Engineering, University of Rome "Tor Vergata", via del Politecnico, 1, 00133 Rome (Italy)

[2] Walter Schottky Institute and Physics Department, Technical University of Munich, 85748 Garching (Germany)

Received 20 October 2003, accepted 13 November 2003
Published online 20 February 2004

PACS 68.55.Hb, 68.55.La, 71.55.Eq, 73.21.Hb, 73.21.La, 77.65.Ly

We theoretically studied the elastic deformation and piezo-electric field in InAs quantum dots and InGaAs quantum wires grown on (N11) GaAs substrates. Particular attention was given to the influence of the substrate orientation on both the volume deformation of the dot and the strain-induced piezo-electric field. The influence of the piezo-electric fields on the electron and hole ground states for a (N11) quantum dot and quantum wire was investigated within the envelope function approach. The exciton effect in a quantum wire was studied.

© 2004 WILEY-VCH Verlag GmbH & Co. KGaA, Weinheim

1 Introduction

Recent advances in growth techniques have made semiconducting quantum dots (QD) grown along [N11] directions a reality [1]. In contrast to the traditional (001) orientation, this geometry enables significant piezo-electric fields in the case of polar crystals with the zinc-blende structure, such as GaAs, AlAs, InAs, and their alloys. These fields lead to a Quantum Confined Stark Effect, which efficiently affects the optical properties of (N11) oriented devices [2]. Consequently, an increasing number of experimental studies has been devoted to such promising systems [3, 4]. Yet, due to the complex geometry of (N11) oriented structures, few theoretical investigations have been performed in this domain.

Heterostructures made of materials with different lattice constants are subjected to elastic deformations. In the case of (001) oriented systems, such deformations have been studied in the framework of both the continuum mechanical model [5, 6] and the valence force field model [7]. Piezo-electric effects which occur in zinc-blende crystals in the presence of a shear deformation were also theoretically investigated for quantum wells (QWs) [8, 9], quantum wires (QWRs) [10] and quantum dots (QDs) [11]. A number of theoretical studies were devoted to the electronic properties of semiconductor nanostructures. They were performed with the use of the envelope function approximations [11], as well as in more refined approaches developed recently, such as the empirical tight-binding method [12, 13] or the empirical pseudo-potential method [14]. The electronic structure of GaAs/AlGaAs (N11) oriented superlattices and unstrained quantum wires was studied in the framework of $\boldsymbol{k} \cdot \boldsymbol{p}$ theory [15, 16]. In a similar approximation the effect of strain on the optical properties of a bulk (N11) oriented system was studied by R. H. Henderson and E. Towe [17]. In this paper, we focus on the influence of strain and piezo-electric fields on the electronic and optical properties of (N11) oriented QDs and

* Corresponding author: e-mail: povolotskyi@ing.uniroma2.it, Phone: +39 06 72597366, Fax: +39 06 2020519

© 2004 WILEY-VCH Verlag GmbH & Co. KGaA, Weinheim

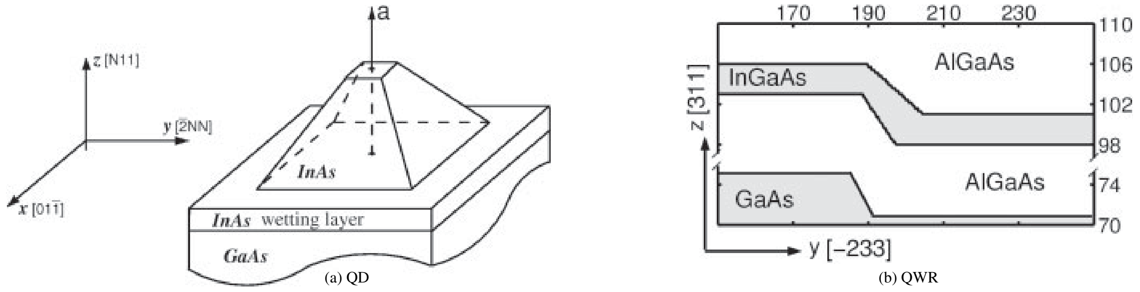

Fig. 1 Schematic drawings of the model heterostructures: a) QD, wetting layer and substrate b) $In_{0.2}Ga_{0.8}As$ QWR, surrounded by an $Al_{0.5}Ga_{0.5}As$ barrier.

QWRs. In addition, we studied the excitonic effect on the optical properties of QWRs. The paper is organized as follows: In section 2 we describe the physical model and methods of numerical calculations, which we apply in section 3 to particular examples of a QWR and QD; the last section 4 summarizes our results.

2 Model and computation

2.1 Model heterostructures

In this study we consider two examples of heterostructures grown on (N11) oriented GaAs substrates, namely a self-assembled QD and a QWR grown on a patterned substrate. The dot has the shape of a symmetric truncated tetrahedral pyramid, standing on a wetting layer, embedded in a GaAs matrix (see Fig. 1a). The two bases of the pyramid are squares of size 10×10 nm and 2×2 nm. The wetting layer thickness is 1 nm, and the dot height is 4 nm. Note that more complex but still pyramidal shapes were reported by Y. Temko et al. for InAs/GaAs dots grown by molecular-beam epitaxy [18].

The considered $In_{0.2}Ga_{0.8}As$ QWR is grown on a (311) oriented GaAs substrate. Similar QWRs were successfully grown and investigated experimentally [19]. Indeed, the growth of an $In_{0.2}Ga_{0.8}As$ quantum well, surrounded by $Al_{0.5}Ga_{0.5}As$ barriers, can be performed on a patterned GaAs substrate, allowing for the appearance of a QWR region near the step of the substrate, as shown in Fig. 1b.

2.2 Elastic deformations and piezo-electric fields

It has been shown that it is possible to directly grow InAs/GaAs QDs by molecular beam epitaxy using the coherent islanding growth effect in highly strained semiconductors [20–22]. High quality side-wall InGaAs/AlGaAs QWRs were observed by means of atomic force microscopy [23, 24].

We calculated the elastic deformation of our model structures by using a continuous medium model [5, 6] thus assuming heterostructures without lattice structure defects. In this approach, we consider the small displacements of the material points $\boldsymbol{u}(\boldsymbol{x})$, which are derived from the local tensor $A_{ij} = \partial u_i/\partial x_j$. Since only the symmetric part of A_{ij} describes "pure" deformations without rotation, the strain tensor ε_{ij} is defined as:

$$\varepsilon_{ij} = \frac{1}{2}(A_{ij} + A_{ji})\,. \tag{1}$$

The energy of the elastic deformation is a quadratic form of ε_{ij}:

$$E = \frac{1}{2}\int_V C_{ijkl}(\boldsymbol{x})\;\varepsilon_{ij}(\boldsymbol{r})\;\varepsilon_{kl}(\boldsymbol{r})\;\mathrm{d}V \tag{2}$$

where C_{ijkl} is the elasticity tensor. Minimization of the elastic energy (Eq. (2)) is equivalent to the mechanical equilibrium condition, written for the case of zero external forces:

$$\frac{\partial\sigma_{ij}}{\partial x_i} = \mathbf{0} \tag{3}$$

© 2004 WILEY-VCH Verlag GmbH & Co. KGaA, Weinheim

where σ_{ij} is the stress tensor, which is related to the strain tensor (Eq. (1)) by Hooke's law:

$$\sigma_{ij} = C_{ijkl}\varepsilon_{kl}\,. \tag{4}$$

The elasticity tensor C_{ijkl} is a bulk material property. It is usually defined in the crystallographic coordinate system but in our case it is more convenient to work in a "growth-oriented" basis whose z-axis is parallel to the growth direction. This new set of coordinate axes in the case of (N11) structures reads:

$$\begin{aligned} \boldsymbol{x} &= [0, \bar{1}, 1] \\ \boldsymbol{y} &= [\bar{2}, N, N] \\ \boldsymbol{z} &= [N, 1, 1] \end{aligned} \tag{5}$$

With this choice, the elasticity tensor must be transformed to the new system (Eq. (5)) according to the rule:

$$C_{ijkl} \;=\; R_{ii'}R_{jj'}R_{kk'}R_{ll'}C_{i'j'k'l'}\,, \tag{6}$$

where R_{ij} is a rotation matrix whose rows are equal to the normalized basis vectors (Eq. (5)). For materials with cubic symmetry, it can be shown that the resulting elasticity tensor has eight zero components among its 21 independent ones. These are namely C_{xxxz}, C_{yyxz}, C_{zzxz}, C_{yzxz}, C_{xxxy}, C_{yyxy}, C_{zzxy}, C_{yzxy}.

As it was mentioned above, we assume a coherent growth, so that all distinct lattices are perfectly matched at the interface [9]. We used the following computational procedure in order to solve Eq. (3), while imposing the lattice matching conditions: We first map a rectangular non-homogeneous simulation grid over the whole structure in such a way that all the material interfaces coincide with the grid lines; we then introduce a "lattice-matching" deformation which transforms any unstrained unit cell of the heterostructure material in order to match it to the reference lattice constant a_r, taken to be equal to the lattice constant of the unstrained substrate:

$$\tilde{\varepsilon}_{ij}(\boldsymbol{r}) = \frac{1}{2}\left(\frac{\partial \tilde{u}_i}{\partial x_j} + \frac{\partial \tilde{u}_j}{\partial x_i}\right) + W(\boldsymbol{r})\,\delta_{ij}\,\frac{a_r - a(\boldsymbol{r})}{a(\boldsymbol{r})} \tag{7}$$

$$W(\boldsymbol{r}) = \begin{cases} 1, & \text{if } \;\boldsymbol{r} \text{ belongs to a deformed layer} \\ 0, & \text{if } \;\boldsymbol{r} \text{ belongs to a substrate} \end{cases} \tag{8}$$

where the $\tilde{\boldsymbol{u}}$ are the displacements additional to the "lattice-matching" deformations and $a(\boldsymbol{r})$ is the equilibrium lattice constant. If, for example, the heterostructure is homogeneous in z direction (QWR structure), then the corresponding derivatives in Eq. (7) vanish. Then the equation of equilibrium (Eq. (3)) takes the following form:

$$\frac{\partial \tilde{\sigma}_{ij}}{\partial x_i} = \mathbf{0}\,, \tag{9}$$

where $\tilde{\sigma}_{ij} \;=\; C_{ijkl}\tilde{\varepsilon}_{kl}$. Eq. (12) is a partial differential equation of the second order with respect to the displacements $\tilde{\boldsymbol{u}}(r)$. It is discretized by using the box integration method and reduced to a linear system represented by a sparse matrix.

The simulation domain includes a part of the substrate and the layers the heterostructure consists of. It has the shape of a rectangular parallelepiped. We assume that the heterostructure is grown on a thick substrate. It has been shown [20, 25] that the minimization of the elastic energy will require a zero strain in the substrate far away from the heterostructure. Therefore, we apply Dirichlet boundary conditions for $\tilde{\boldsymbol{u}}(r)$ at the plane that separates the simulation domain from the rest of the substrate. The necessary depth of the strained substrate region to be considered in order to get convergent results was found to be about 20–40 nm. The cap layer that surrounds the QD or QWR is also considered to be strained. At its boundary planes we apply von Neumann boundary conditions in order to consider the case of zero external stress acting on the heterostructure.

© 2004 WILEY-VCH Verlag GmbH & Co. KGaA, Weinheim

The piezo-electric polarization is linearly related to strain

$$P_i = e_{ijk} \varepsilon_{jk} , \tag{10}$$

where the e_{ijk} are the piezo-electric tensor components. Due to the cubic symmetry of zinc-blende crystals, the non-zero e_{ijk}s in the crystallographic coordinate system are only related to shear deformations. In the coordinate system (Eq. (5)), however, diagonal components of the strain tensor may also contribute to the piezo-electric polarization. In this study, we neglect the converse piezo-electric effect [26], and use the polarization $\boldsymbol{P}$ to obtain the electric potential from the Poisson equation

$$-\nabla(\kappa \nabla \varphi) = -\nabla \boldsymbol{P} , \tag{11}$$

where κ is the dielectric constant. Here, we consider that there are no free charges in the structure, thus the built-in electric field may originate only from a piezo-electric charge $\rho_{\text{piezo}} = -\nabla \boldsymbol{P}$.

2.3 Electron and hole eigenstates

We investigated the electron and hole eigenstates in our model QD structures within the effective mass approximation (EMA), and considered only the lowest conduction band for electrons and the highest valence band for holes. A similar approach was used by Grundmann and co-workers [27] for the description of electron and hole states in the InAs/GaAs(001) strained QD. They considered longitudinal and transversal hole effective mass that corresponds to the case of a biaxial strain, namely $\varepsilon_{xx} = \varepsilon_{yy} \neq \varepsilon_{zz}, \varepsilon_{xy} = \varepsilon_{yz} = \varepsilon_{zx} = 0$ [28]. Strain-induced shifts of the conduction band depend only on the hydrostatic part of the strain: $\delta E_c = -a_c \operatorname{Tr}(\varepsilon_{ij})$ where a_c is the deformation potential. Here, the influence of strain on the electron effective mass is neglected and, therefore, an isotropic bulk effective mass is considered. The band shifts and the effective mass tensor for the highest valence band are obtained from the Bir-Pikus 6×6 $\boldsymbol{k} \cdot \boldsymbol{p}$ Hamiltonian [17, 28]. In our approach, the hole effective mass is position dependent and has both diagonal and off-diagonal components. At a given $\boldsymbol{r}$ point, $m^*(\boldsymbol{r})$ is the effective mass of the bulk semiconductor, subjected to the homogeneous strain $\varepsilon(\boldsymbol{r})$. The electron and hole eigenstates were obtained as the solutions of the one-particle Schrödinger equation:

$$\left(-\frac{\hbar^2}{2} \frac{\partial}{\partial x_i} \frac{1}{m^*{}_{ij}(\boldsymbol{r})} \frac{\partial}{\partial x_j} + V_\varepsilon(\boldsymbol{r}) + q\varphi(\boldsymbol{r}) \right) \psi = E\psi \tag{12}$$

where $m^*, q, V_\varepsilon, \varphi$ are the conduction (valence) band effective mass, electron (hole) charge, conduction (valence) band edge energy and piezo-electric potential, respectively. Eq. (12) is discretized over a rectangular non-homogeneous grid by using the box integration method. The problem is then reduced to the diagonalization of a Hermitian sparse matrix.

The theoretical approach described above has been implemented into the next**nano**^{3} software package [29]. The necessary material parameters were taken from [30].

2.4 Excitonic effects in QWRs

An accurate description of the optical properties of a nanostructure should take into the excitonic effect. The case of a QWR is simpler than of the case of a QD because we can reduce the dimension of the problem using the approximation of the separable motion along the "quantized" two-dimensional subspace and along the wire. The exciton was described within the framework of the variational approach [31, 32]. We start from the wave function that describes the relative motion of the electron-hole pair, written in the form of separable coordinate variables

$$\psi_{\text{ex}}(\boldsymbol{r}_e^{\|}, \boldsymbol{r}_h^{\|}, z) = \chi_e(\boldsymbol{r}_e^{\|})\, \chi_h(\boldsymbol{r}_h^{\|})\, g(z) , \tag{13}$$

where $\boldsymbol{r}_e^{\|}$, $\boldsymbol{r}_h^{\|}$ are the in-plane positions of electron and hole, $z = z_e - z_h$ is the distance between particles in the "non-quantized" direction.

© 2004 WILEY-VCH Verlag GmbH & Co. KGaA, Weinheim

The functions $\chi_e(\boldsymbol{r}_e^{\|})$ and $\chi_h(\boldsymbol{r}_h^{\|})$ are linear combinations of the electron/hole eigenfunctions $\psi_e^i(\boldsymbol{r}_e^{\|})$ and $\psi_h^i(\boldsymbol{r}_h^{\|})$, that are solutions of the single-particle Schrödinger equation (Eq. (12)).

$$\chi_e = \sum_{i=0}^{N_e} c_e^i \psi_e^i \tag{14}$$

$$\chi_h = \sum_{i=0}^{N_h} c_h^i \psi_h^i \tag{15}$$

$$g(z) = \left(\frac{2}{a^2\pi}\right)^{1/4} \exp\left(-\frac{z^2}{a^2}\right) \tag{16}$$

N_e and N_h refer to the number of functions included in the expansions (Eqs. (14, 15)). Parameter a and the coefficients c_e^i, c_h^i are the variational parameters. As follows from Eqs. (14, 15) we do not neglect the contribution of the excited electron and hole states [33].

The exciton wave function (Eq. (13)) gives the minimum to the exciton energy that can be expressed as a sum of single particle energies ($\tilde{E}^e$, $\tilde{E}^h$), electrostatic interaction energy (H^{Coul}) and kinetic energy of the relative motion along the wire (H^{kin}):

$$E_{\text{ex}} = \tilde{E}_e + \tilde{E}_h + H^{\text{Coul}} + H^{\text{kin}} \tag{17}$$

$$\tilde{E}_e = \sum_{i=1}^{N_e} |c_e^i|^2 \, E_e^i \tag{18}$$

$$\tilde{E}_h = \sum_{i=1}^{N_h} |c_h^i|^2 \, E_h^i \tag{19}$$

$$H^{\text{Coul}} = -\int\limits_{\boldsymbol{r}_e^{\|},\boldsymbol{r}_h^{\|},z} \frac{|\psi_{ex}(r_e^{\|},\boldsymbol{r}_h^{\|},z)|^2}{\kappa\sqrt{(\boldsymbol{r}_e^{\|}-\boldsymbol{r}_h^{\|})^2+z^2}} \, \mathrm{d}\boldsymbol{r}_e^{\|}\, \mathrm{d}\boldsymbol{r}_h^{\|}\, \mathrm{d}z \tag{20}$$

$$H^{\text{kin}} = \frac{\hbar^2}{2\mu a^2} \tag{21}$$

$$\frac{1}{\mu} = \frac{1}{\tilde{m}_{zz}^e} + \frac{1}{\tilde{m}_{zz}^h}; \qquad \frac{1}{\tilde{m}_{zz}^{e,h}} = \left\langle \chi_{e,h} \left| \frac{1}{m_{zz}^{e,h}} \right| \chi_{e,h} \right\rangle \tag{22}$$

where κ is the dielectric constant considered to be the same for all materials. Here we neglect the image charge effect, exchange interaction and used an averaged value for the effective mass m_{zz}. Minimization of the exciton energy (Eq. (17)) was performed using the Nelder-Mead simplex algorithm [34]. The starting values of the expansion coefficients $c_{e,h}^j$ for minimization were chosen as

$$c_{e,h}^i = \begin{cases} 1, & i = 0 \\ 0, & i = 1, 2, 3, \ldots, N_{e,h} \end{cases}. \tag{23}$$

thus considering excited states contribution to be small comparatively to the contribution of the ground state. We found that it is sufficient to put $N_e = N_h = 2$ in order to get the convergence level for the exciton binding energy better than 0.05 meV.

The oscillator strength of the optical dipole transition was estimated by the following formula [32]:

$$f \propto |\langle \chi_e \mid \chi_h \rangle|^2 \, |g(0)|^2 \,. \tag{24}$$

3 Results and discussion

3.1 Strain pattern

Contour plots of the strain tensor components for the QD, grown on a (211) oriented substrate, and the QWR, grown on a (311) oriented substrate, are shown in Fig. 2. The results are qualitatively the

© 2004 WILEY-VCH Verlag GmbH & Co. KGaA, Weinheim

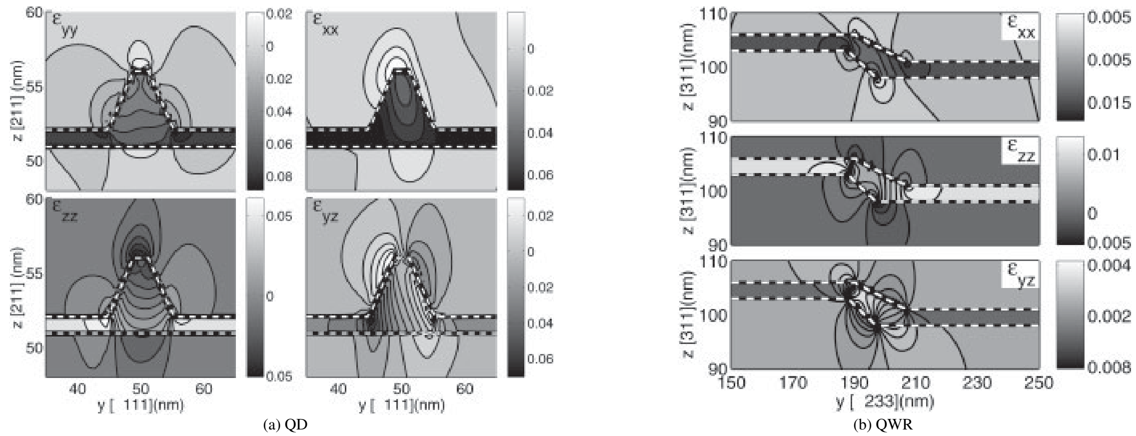

Fig. 2 Contour plot of the strain tensor components. a) Distribution over a cross section of the QD. The section plane is parallel to the $(\bar{1}11)$ crystallographic plane. The QD symmetry axis a (see Fig. 1a) belongs to the section. b) Distribution over a cross section of the QWR. The section plane is parallel to the $(0\bar{1}1)$ crystallographic plane. White dashed lines indicate heterointerfaces.

same for any [N11]-like direction. We plot diagonal (ε_{xx}, ε_{yy}, ε_{zz}) and an off-diagonal (ε_{yz}) component. The plots indicate that both the QD/QWR layer materials are compressed in the x and y directions (ε_{xx}, ε_{yy} are negative), in agreement with the relative values of the lattice constants of InAs and GaAs. As for the ε_{zz} component, the situation in the QD and QWR is quite different. Namely, in the QD the two-dimensional wetting layer is tensile-strained in the growth direction, but the pyramid is compressively strained because its lateral faces are also subjected to compression. In the QWR structure, the ε_{zz} is always negative. Interestingly, the strain distribution in the QD is not symmetric, despite of the symmetric QD shape (Fig. 2a). The loss of symmetry is due to the fact that the [N11] and $[\bar{2}NN]$ directions do not coincide with the high-symmetry axes of a cubic crystal. In both structures the strain pattern is homogeneous only far from the QWR or QD region, where the structure is similar to a quantum well. In this region the atomic displacements in the directions parallel to the substrate plane (ε_{xx} and ε_{yy} components) are such that the in-plane lattice constants of the strained material are equal to the lattice constant of the substrate. The atomic displacements in the growth direction (ε_{zz} component) and additional shears (ε_{zx} and ε_{zy}) have to minimize the elastic energy (Eq. (2)). In the QWR and QD region the displacements of the atoms are such that the lattice constant is matched at the interfaces which are oriented arbitrarily with respect to the substrate plane. On the other hand, the elastic energy minimization affects all components of the strain tensor. Therefore, the strain distribution in this region is not homogeneous.

3.2 Piezoelectricity

Due to the nature of the piezo-electric effect, the sign of the piezo-electric charge depends on the atomic composition of the interfaces [2]. We thus have to distinguish between the substrate's Ga planes, referred to as (N11)A-plane, and the As planes, referred to as (N11)B-plane. From the computational point of view, these two cases differ in the sign of the piezolectric tensor e_{ijk} (see Eq. (10)). There are two reasons for the existence of the piezo-electric charge, namely, the discontinuity of the piezo-electric constant at the interfaces and the non-zero gradient of strain. This explains the big charge density at the interfaces, that corresponds to a surface charge. In addition, there is a volume charge inside the QD/QWR, where the strain is highly non-homogeneous. Previously, a piezo-electric quadrupole has been reported by Stier et al. [11] for (100) oriented QDs. In contrast to that, the (N11) oriented dot of the same shape, has a piezo-electric charge with a dipole symmetry [35] (see Fig. 3). It is worth to emphasize the existence of two charged interface planes in the case of the (211) oriented QD. Far from the QD region these planes have equal in absolute value and different in sign

© 2004 WILEY-VCH Verlag GmbH & Co. KGaA, Weinheim

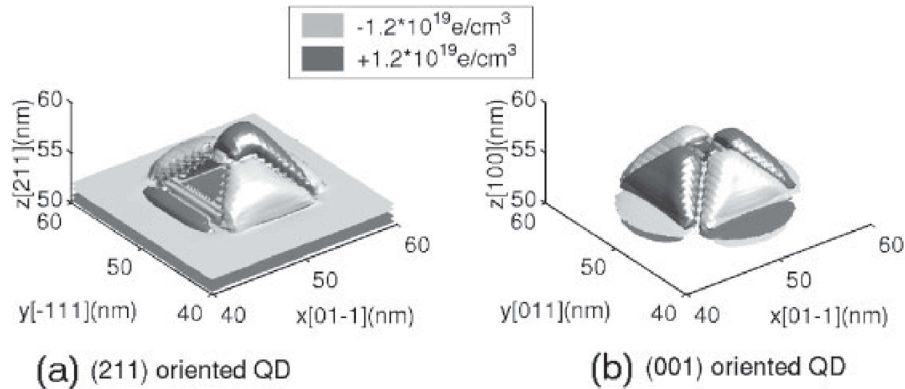

Fig. 3 Piezo-electric charge density. Comparison between a) (211) oriented QD and b) (100) oriented QD.

piezoelectric charge. Such a charge distribution is typical of (N11) oriented quantum well structures [8].

In order to show how the piezo-electric field affects the band structure, we plot the valence band profile of the QD structure with and without taking into account the piezo-electric effect (Fig. 4). One can see that the piezo-electric field acts in a different way, depending on the substrate orientation. For example, in the case of a QWR grown on (311)A substrate, the top of the valence band of InGaAs is shifted away from the substrate (see Fig. 4b). In the opposite case, corresponding to (311)B substrate, the band's top is shifted towards the substrate.

3.3 Electronic and optical properties

3.3.1 Quantum dot

Our study enables us to consider two effects on the electron and hole states, namely, the effect of strain and the effect of the piezo-electric charge. The effect of strain in our model does not depend on

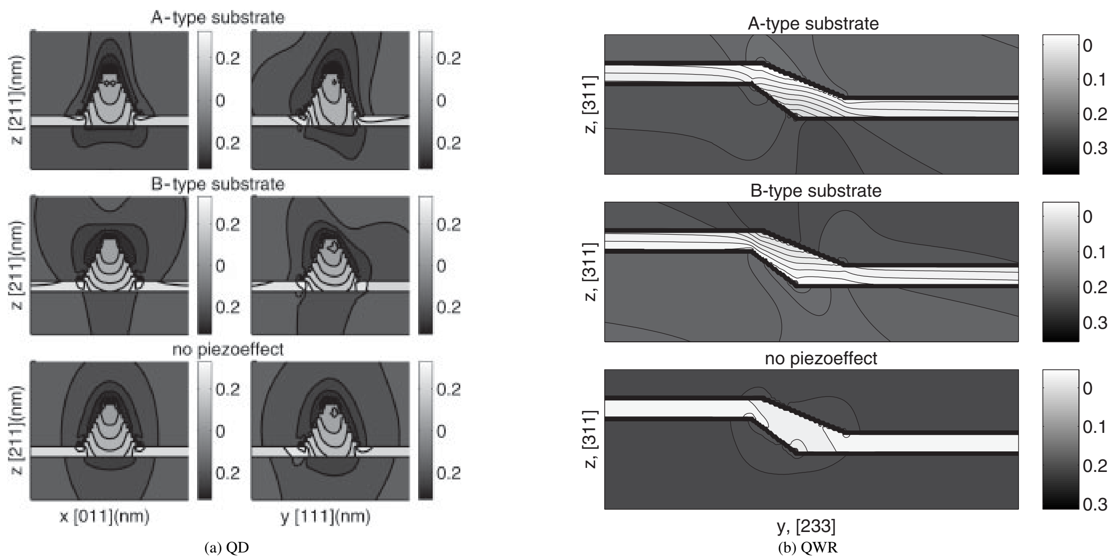

Fig. 4 Contour plot of the valence band edge profile calculated for three cases: A-type substrate, B-type substrate and neglecting piezo-electric effects. The colorbar units are eV. a) Two perpendicular cross sections of the QD grown on (211) oriented substrate. The section planes contain the QD symmetry axis *a* (see Fig. 1a). b) Cross section of the QWR grown on (311) oriented substrate.

© 2004 WILEY-VCH Verlag GmbH & Co. KGaA, Weinheim

Table 1 Fundamental transition energy calculated for (N11) oriented QDs (eV).

growth direction	no piezo-effect	(N11)A	(N11)B
[111]	1.254	1.262	1.241
[211]	1.241	1.243	1.233
[311]	1.224	1.226	1.221
[100]	1.205	1.205	1.205

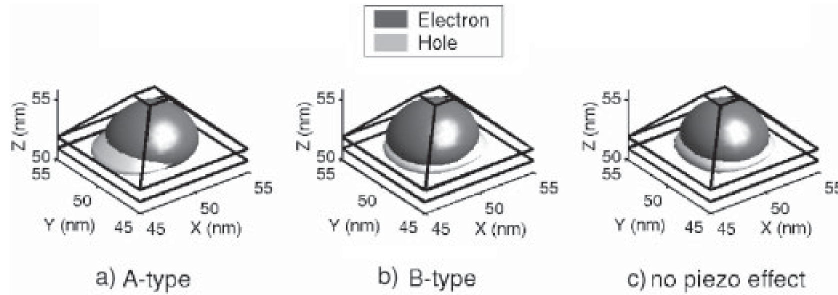

Fig. 5 Isosurface of the squared modulus of the electron/hole ground state wave function in the QD. a), b) Piezo-electric effect is taken into account for A- and B-type substrates, respectively; c) Piezo-electric effect is neglected.

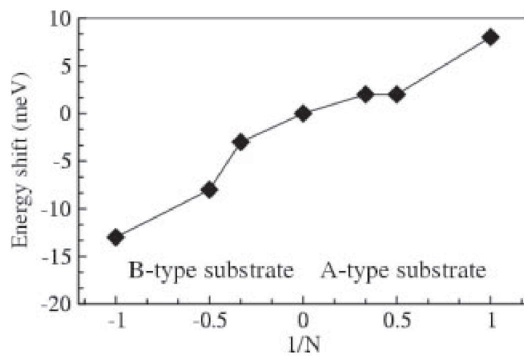

Fig. 6 The fundamental transition energy shift due to the piezo-electric effect. Axis of abscissae indicates the substrate orientation: positive numbers correspond to (N11)A substrate, negative numbers to (N11)B.

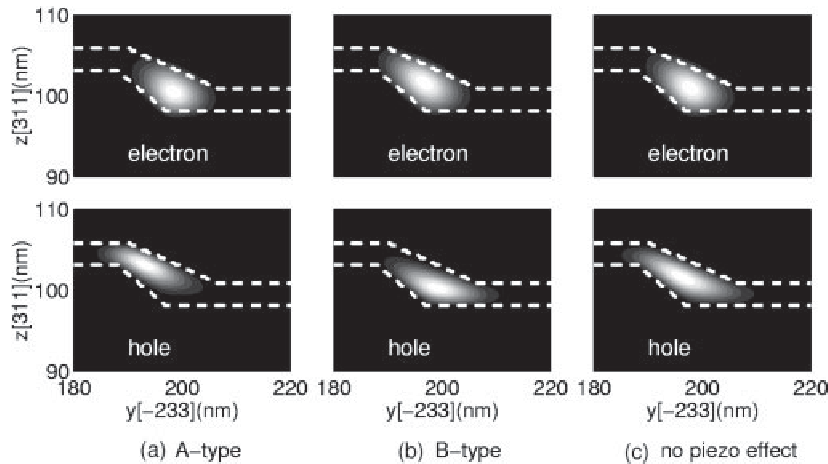

Fig. 7 Contour plots of squared modulus of the electron/hole ground state wave function in the QWR. a), b) Piezo-electric effect is taken into account for A- and B-type substrates, respectively; c) Piezo-electric effect is neglected. Dashed lines indicate heterointerfaces.

© 2004 WILEY-VCH Verlag GmbH & Co. KGaA, Weinheim

the substrate termination type, but the piezo-effect does. In order to investigate the role of the piezo-electric field, we calculated the fundamental transition energy without any piezo-electric field and with the field, for both the A and B substrate type (see Table 1). We found that the fundamental transition energy can either be reduced or enlarged by the piezo-electric field. The corresponding shift is plotted in Fig. 6. We see that the effect has different sign depending on the substrate termination, and different magnitude which increases as the [N11]-growth direction deviates from [100] towards [111] direction. The energy shift is less than 1meV for (100) oriented structures and reaches a value of more than 10meV for (111) orientation. As one can see from a $|\psi(\boldsymbol{r})|^2$-function plot (Fig. 5), the electron and hole ground state wave functions are shifted away due to strain even without piezo-electric field (see band diagram in Fig. 4a). The piezo-electric effect can enlarge or reduce this spatial separation. Its influence on the eigenfunctions is larger in the case of (N11)A substrate then in the case of (N11)B substrate. Also, the transition energy for A substrate is larger than for B substrate. This evidences that the positive energy shift due to the effect of quantization dominates over the negative shift due to the band bending. Since even without piezo-electric field electron and hole are separated, the energy shift due to the piezo-electric effect changes its sign if the field direction is inverted.

3.3.2 Quantum wire

We calculated the eigenenergies and eigenfunctions of electron and hole in the QWR structure taking into account piezo-electric effect for both substrate terminations as well as neglecting it. Modulus squared of the electron and hole wave functions of the ground state are shown in Fig. 7. Due to the non-symmetric shape of the QWR, the electron and hole wave functions are stronger separated in the case of A-terminated substrate than in the case of B-terminated substrate. One can see in Table 2 that the piezo-electric field reduces both the transition energy and the overlap integral between electron and hole $|\langle\varphi_e \mid \varphi_h\rangle|^2$, irrespective of the substrate termination type. This can be explained by the fact that our QWR is large enough and the strain is more homogeneous in comparison to the QD.

It is interesting to compare the exciton binding energy with and without piezo-electric field. We see that the piezo-electric field reduces the exciton binding energy. The reduction is different for A and B substrate termination. Namely, in the case of the A-terminated substrate, where we have stronger electron/hole separation due to the field, the exciton binding energy is reduced by 10%. In the case of the opposite field orientation, the reduction is less then 1%.

Similarly the piezo-electric field affects the oscillator strength. If we neglect the excitonic effect, then the oscillator strength is proportional to the overlap integral between electron and hole. In this case the strength is reduced by 35% in the case of (311)A substrate and by 8% in the case of (311)B substrate. The excitonic interaction leads to attraction of the hole to the electron. Therefore, the relative reduction of the oscillator strength becomes less, namely 32% and 5%, respectively.

Table 2 Values of inter-band transition energy $E_e - E_h$, single particle overlap integral $|\langle\varphi_e \mid \varphi_h\rangle|^2$, exciton binding energy, modulus squared of the exciton wave function $|g(0)|^2$, overlap between electron and hole wave functions $|\langle\chi_e \mid \chi_h\rangle|^2$ and oscillator strength f.

	A-type substrate	B-type substrate	no piezo-effect
single particle properties			
$E_e - E_h$, eV	1.467	1.475	1.477
$\|\langle\varphi_e\|\varphi_h\rangle\|^2$	0.55	0.78	0.85
exciton properties			
$\|\langle\chi_e\|\chi_h\rangle\|^2$	0.61	0.81	0.85
E_b, meV	10.80	12.15	12.20
$\|g(0)\|^2$, nm^{-1}	0.043	0.045	0.045
f, a.u.	26	36	38

© 2004 WILEY-VCH Verlag GmbH & Co. KGaA, Weinheim

The time resolved photoluminescence experiments, in which the influence of piezo-electric charge on the optical properties of QWRs and QDs was studied, have been performed recently [2, 36]. In these experiments the time-shift of the fundamental transition energy was detected. The energy shift was explained as a result of the piezo-electric field screening due to the photo-injected non-equilibrium carriers. The detailed comparison between experimental results and calculations will be presented elsewere [37].

4 Conclusions

We investigated the structural and electronic properties of nanostructures grown on (N11) oriented GaAs substrates. We obtained a non-symmetric strain pattern, as well as an increasing piezo-electric field for high index orientations. Our calculations demonstrate that by varying the growth direction and the substrate termination type, it is possible to tailor the built-in electric field, and, therefore, the optical properties of such QDs and QWRs. Hence, the electron and hole wave functions can be engineered in such a way that we can have a quantum system where electron and hole, being in the ground state, are spatially separated. Such systems can be used for quantum information processor applications [38].

Acknowledgements We acknowledge the Office of Naval Research and the PAIS-PIE project for the financial support. We acknowledge many useful discussions with Dr. Stefano Sanguinetti and Prof. Massimo Gurioli.

References

[1] P. Gonzáles-Borrero, D. Lubyshev, E. Marega, Jr., E. Petitprez, and P. Basmaji, J. Cryst. Growth **169**, 424 (1996).
[2] S. Sanguinetti, M. Gurioli, E. Grilli, M. Guzzi, and M. Henini, Appl. Phys. Lett. **77**, 1982 (2000).
[3] S. Marcinkevičius, J. Siegert, R. Leon, B. Čechavičius, B. Magness, W. Taylor, and C. Lobo, Phys. Rev. B **66**, 235314 (2002).
[4] S. Fréchengues, N. Bertru, V. Drouot, B. Lambert, S. Robinet, and S. Loualiche, Appl. Phys. Lett. **74**, 3356 (1999).
[5] C. Pryor, M.-E. Pistol, and L. Samuelson, Phys. Rev. B **56**, 10404 (1997).
[6] B. Jogai, J. Appl. Phys. **88**, 5050 (2000).
[7] P. Keating, Phys. Rev. 1**45**, 637 (1966).
[8] D. Smith and C. Mailhiot, Phys. Rev. B **63**, 2717 (1988).
[9] L. De Caro and L. Tapfer, Phys. Rev. B **48**, 2298 (1993).
[10] L. De Caro and L. Tapfer, Phys. Rev. B **51**, 4381 (1995).
[11] O. Stier, M. Grundmann, and D. Bimberg, Phys. Rev. B **59**, 5688 (1998).
[12] A. Di Carlo, Semiconductor Science and Technology **18**, R1 (2003).
[13] G. Klimeck, F. Oyafuso, R. C. Bowen, and T. B. Boykin, Superlattices Microstruct. **31**, 171 (2002).
[14] A. W. L. Wang and A. Zunger, Phys. Rev. B **62**, 12963 (2000).
[15] J.-B. Xia, Phys. Rev. B **43**, 9856 (1991).
[16] S.-S. Li and J.-B. Xia, Phys. Rev. B **50**, 8602 (1994).
[17] R. Henderson and E. Towe, J. Appl. Phys. **78**, 2447 (1995).
[18] T. S. Y. Temko and K. Jacobi, Appl. Phys. Lett. **82**, 2142 (2003).
[19] R. Nötzel, M. Ramsteiner, Z. Niu, H.-P. Schönher, L. Däweritz, and K. H. Ploog, Appl. Phys. Lett. **70**, 1578 (1997).
[20] L. A. Zepeda-Ruiz, R. I. Pelzel, B. Z. Nosho, W. H. Weinberg, and D. Maroudas, J. Appl. Phys. **90**, 2689 (2001).
[21] S. Guha, A. Madhukar, and K. Rajkumar, Appl. Phys. Lett. **57**, 2110 (1990).
[22] S.-Z. Chang, T.-C. Chang, and S.-C. Lee, J. Appl. Phys. **73**, 4916 (1993).
[23] R. Nötzel, U. Jahn, Z. Niu, A. Tranpert, J. Fricke, and H.-P. Schönherr, Appl. Phys. Lett. **72**, 2002 (1998).
[24] R. Nötzel, M. Ramsteiner, J. Menninger, A. Tranpert, H.-P. Schönherr, L. Däweritz, and K. H. Ploog, J. Appl. Phys. **80**, 4108 (1996).
[25] C. G. Van de Walle, Phys. Rev. B **39**, 1871 (1989).
[26] T. Bahder, Phys. Rev. B **51**, 10892 (1995).

© 2004 WILEY-VCH Verlag GmbH & Co. KGaA, Weinheim

[27] M. Grundmann, O. Stier, and D. Bimberg, Phys. Rev. B **52**, 11969 (1995).
[28] C.-P. Chao and S. Chuang, Phys. Rev. B **46**, 4110 (1992).
[29] next**nano**^{3} device simulation package, see website http://www.nextnano.de.
[30] I. Vurgaftman, J. R. Meyer, and L. R. Ram-Mohan, J. Appl. Phys. **89**, 5815 (2001).
[31] A. Kiselev and U. Rössler, Semiconductor Science and Technology **11**, 203 (1995).
[32] F. Madarasz, F. Szmulowicz, F. Hopkins, and D. Dorsey, Phys. Rev. B **49**, 13528 (1994).
[33] M. Szymanska, P. Littlewwod, and R. Needs, Phys. Rev. B **63**, 205317 (2001).
[34] J. A. Nelder and R. Mead, Comput. J. **7**, 308 (1965).
[35] M. Povolotskyi, A. Di Carlo, P. Lugli, S. Birner, and P. Vogl, to be published in IEEE transactions on Nanotechnology.
[36] D. Alderighi, M. Zamfirescu, M. Gurioli, A. Vinattieri, M. Colocci, S. Sanguinetti, M. Povolotskyi, A. D. Carlo, P. Lugli, and R. Ntzel, phys. stat. sol. (c) **0**, 1433 (2003).
[37] D. Alderighi, M. Zamfirescu, A. Vinattieri, M. Gurioli, S. Sanguinetti, M. Povolotskyi, J. Gleize, A. D. Carlo, and P. Lugli, submitted to Appl. Phys. Lett.
[38] S. De Rinaldis, I. D'Amico, and F. Rossi, Appl. Phys. Lett. **81**, 4236 (2002).

© 2004 WILEY-VCH Verlag GmbH & Co. KGaA, Weinheim